Experimental Study of the Liquid/Vapor Phase Change in a Porous Media of Two-Phase Heat Transfer Devices

Riadh Boubaker, Souad Harmand, Vincent Platel

Applied Thermal Engineering 143 (2018) 275–282

Experimental study of the liquid/vapor phase change in a porous media of two-phase heat transfer devices

Riadh Boubaker[a,*], Souad Harmand[a], Vincent Platel[b]

[a] Laboratoire d'Automatique, de Mécanique et d'Informatique industrielles et Humaines (LAMIH), Université de Valenciennes et du Hainaut-Cambrésis (UVHC) Le Mont Houy, F59313 Valenciennes CEDEX 9, France

[b] Univ Pau & Pays Adour, Laboratoire de Thermique, Energétique et Procédés-IPRA EA1932, Pau, France

ARTIC LE I NFO

Keywords:
Phase change
Porous media
Capillary pumping
Heat transfer

ABSTRAC T

The study presents an experimental examination of heat and mass transfer with phase change in a porous media composed of copper foam. The aim of the study involves separately examining the effect of the adverse hydrostatic head, subcooling at the wick inlet and wick properties (porosity and average pore diameter) on the heat and mass transfer inside porous media. The experimental results indicate that an increase in the adverse hydrostatic head from $\Delta h = 0.5$ cm to $\Delta h = 2$ cm increases the casing temperature of 5 °C for low heat loads and 40 °C for high heat loads owing the vapor breakthrough toward the wick inlet. The results also suggest that the heat transfer coefficient and the critical heat flux are reduced by approximately 27% (for a heat load of 106 W) and 17%, respectively for the same adverse hydrostatic head variation. The increase in the subcooling at the wick inlet reduces the thermal performance of the evaporator. With respect to wick property effects, the results indicate that the porosity and average pore diameter significantly impact the phase change phenomenon inside the porous wick and the casing temperature. There are optimal values of porosity and average pore diameter leading to the best thermal performance of the capillary evaporator.

1. Introduction

The phase change phenomenon in porous media occupies an important role in several applications, and particularly in heat transfer systems such as Capillary Pumped Loop (CPL) and Loop Heat Pipe (LHP) [1–4]. Passive two-phase heat transfer devices use fluid circulation and phase change properties in a porous medium to transfer high amounts of heat over distances of a few meters from a hot source to a cold source. As shown in Fig. 1, they are composed of an evaporator, a condenser, a reservoir (a compensation chamber) and vapor and liquid lines.

The evaporator is the key element of such devices, which absorbs the heat dissipated by the hot source (electronic components). The generated capillary pressure in the pores is responsible for the fluid circulation in the complete loop. As shown in Fig. 2, the evaporator consists of a porous structure called wick that is tightly enveloped by a metal container.

Over the last decade, several efforts focused on simulating the phase change phenomenon inside the porous wick of capillary evaporators. Kaya and Goldak [5] numerically examined heat and mass transfers in the porous structure of an LHP. The proposed mathematical model is inspired from a study by Demidov and Yatsenko [6]. They showed the existence of a vapor pocket when the fluid temperature exceeds the saturation temperature by a few degrees. Huang [7] also developed an unsteady model to study heat and mass transfers with phase change in the porous wick of an evaporator of a CPL.

* Corresponding author.
E-mail addresses: boubakker.riadh@yahoo.fr (R. Boubaker), souad.harmand@univ-valenciennes.fr (S. Harmand), vincent.platel@univ-pau.fr (V. Platel).

DOI : 10.1016/j.applthermaleng.2018.07.058

Nomenclature

V	voltage, V
I	current, A
C_p	specific heat, J kg^{-1} K^{-1}
h	heat transfer coefficient, W m^{-2} K^{-1}
S	cross section, m^2
L_v	latent heat, J kg^{-1}
p	pressure, Pa
t	time, s
T	temperature, K
K	permeability, m^2
r_m	meniscus curvature, m
r_p	pore radius, m
g	gravitational acceleration, ms^{-2}

Greek symbols

Δp	pressure drop, Pa
Δh	adverse hydrostatic head, cm
σ	surface tension, N m^{-1}
λ	thermal conductivity, W m^{-1} K^{-1}
μ	dynamic viscosity, kg m^{-1} s^{-1}
ρ	density, kg m^{-3}
ϕ	heat flux, W
θ	contact angle, rad
$\dot{m}$	mass flow rate, kg s^{-1}
Ω	volume, m^3

Subscripts

ℓ	liquid
v	vapor
s	solid
eff	effective
cap	capillary
sat	saturation
C	casing
R	reservoir
in	inlet
o	outlet
W	wick
p	parasitic
sens	sensible

In the study, the porous wick was divided into the following three regions: a liquid zone, vapor zone and two-phase zone where the phase change occurs. The results showed that the thickness of the liquid/vapor interface is non-zero. Xuan et al. [8] simulated the coupled heat and mass transfer with phase change in a global CPL evaporator by using a two-dimensional (2D) transient model based on the lattice Boltzmann method. Masahito Nishikawara and Hosei Nagano [9] investigated the effect of adding a microgap between the casing and porous wick on capillary evaporator performance. The results indicated that an optimal gap distance exists leading to a high thermal coefficient. Mottet and Prat [10] investigated heat and mass transfer with phase change in a bidispersed capillary structure characterized by a bimodal pore size distribution using a mixed pore network model. The simulations demonstrated that the bidispersed wick exhibits better thermal performance than a monodispersed wick for high heat loads. Boubaker et al. [11] presented an unsteady mathematical model of a flat CPL evaporator. The developed model describes heat and mass transfers as well as phase change phenomenon within the porous wick. Subsequently, the evaporator model was coupled with a complete loop model [12,13]. The effects of applied power, working fluid and porous wick properties on the thermal performance of a capillary pumped loop and vapor pocket behavior inside the porous wick were analyzed. Z.M. Wan et al. [14] presented a 2D model to analyze heat and mass transfer in a miniature flat capillary pumped loop evaporator with a fully saturated wick. Wu et al. [15] investigated the impact of the bayonet tube on the phase change in the porous wick of a capillary evaporator. The results indicate that the bayonet tube decreases the temperature inside the porous wick and reduces the risk of evaporator failure. Le et al. [16] developed a 2D pore network model to describe heat and mass transfer in an unsaturated porous wick and to examine the impact of microstructural properties on the vapor pocket pattern. Three dimensional (3D) models were also developed to study the liquid/vapor phase change in capillary evaporators with a fully saturated wick [17–20] and unsaturated wick [21].

Although numerical studies focused on analyzing the phase change inside a porous wick, there is a paucity of experimental studies that examine heat and mass transfers inside a capillary evaporator in the case where it is decoupled from the rest of the CPL/LHP components owing to the complexity of the coupled physical phenomenon that occurs inside the wick. Liao and Zhao [22,23] performed an experiment to investigate mass and heat transfer processes in a rectangular porous structure in a stationary regime. Experimental results indicated the existence of a vapor pocket that develops inside the porous wick. The authors also demonstrated that the temperature field in the porous medium depends on gravity losses, subcooling at the wick inlet and pore radius. Cao et al. [24] investigated heat and mass processes in bidispersed wick structures of a capillary evaporator. The results indicated that the use of bidispersed wicks significantly improves the thermal performance of capillary evaporators. An experimental study

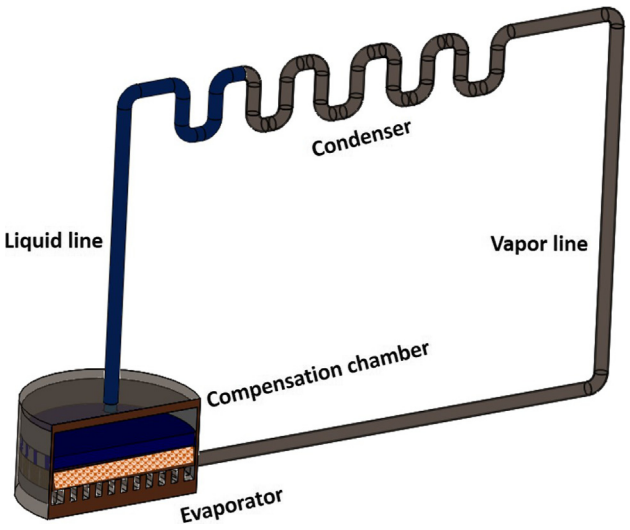

Fig. 1. LHP design.

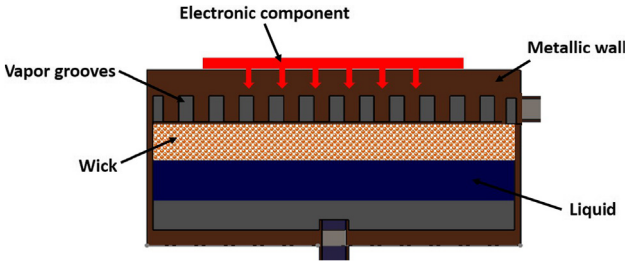

Fig. 2. Capillary evaporator.

was conducted by Coquard [25] to visualize the phenomenon of vaporization in a porous medium. The porous wick consists of a monolayer of steel beads. It should be noted that the study was limited to verify the formation of a vapor pocket inside the porous wick. Odagiri et al. [26] performed a visual study to investigate the liquidvapor phase change at the wick surface of an LHP evaporator. The impact of the wick material and width of the vapor grooves on the thermal performance of the capillary evaporator was examined.

Several mechanisms of the capillary evaporator are still not adequately understood to date and require further investigations. The objective of the present study is to gain a better understanding of the phase change phenomenon inside a porous wick. The novelty of this study lies in separately analyzing the effect of gravity pressure drop, subcooling at the wick inlet and wick properties (porosity and average pore diameter) on the heat and mass transfer inside the porous wick. The impact of the adverse hydrostatic head on the vapor pocket behavior is also visualized.

2. Capillary two-phase loop operating principles

The liquid is subcooled uniformly in the wick prior to the initial time corresponding to the beginning of the application of the heat load. A heat load that isdissipated by electronic components is supplied to the evaporator casing and is transferred to the working fluid in the wick by conduction through the porous structure. This increases liquid temperature with respect to time until it reaches the saturation temperature of the vapor inside the grooves. Evaporation subsequently commences at the hottest point of the upper surface of the wick, and this is the contact surface with the evaporator casing. The vapor is evacuated through the vapor grooves. The subcooled liquid motion is pumped by capillarity through the condenser, liquid line and reservoir to reach the evaporator inlet.

Therefore, capillary pumping operation plays an essential role in ensuring the smooth operation of the capillary two-phase loop. This corresponds to the curvature of the liquidvapor interface that is composed of several menisci and generates the capillary pressure jump Δp_{cap} that is responsible for the circulation of the fluid in the porous wick.

The overpressure of the vapor above the liquid/vapor interface leads to its migration toward the grooves. The liquid is pumped into the wick by the depression that prevails under the meniscus of the liquid/vapor interface, and this subsequently ensures the continuity of the vaporization process.

Assuming a spherical liquid/vapor interface, the capillary pressure jump is inversely proportional to the curvature radius based on the Young-Laplace's law:

$$\Delta p_{cap} = p_v - p_\ell = \frac{2\sigma}{r_m} = \frac{2\sigma\cos\theta}{r_p} \quad (1)$$

where r_p denotes the pore radius and θ denotes t the contact angle between the liquid and the wick. For a perfectly wetting fluid, the contact angle is zero. In the steady state, the capillary pressure jump must exactly compensate the pressure drop in the condenser, wick, grooves, and liquid and vapor lines.

3. Study of a capillary evaporator

3.1. Experimental setup

The operation of capillary two-phase loops presents complex couplings of the thermal and hydrodynamic mechanisms owing to the interactions between the loop components (reservoir, evaporator, condenser,and vapor and liquid lines), and this leads to simultaneous variations in subcooling and pressure drops across the evaporator. The couplings significantly influence the phenomenon of liquid/vapor phase change inside the porous wick and considerably complicate the understanding of the phenomenon.

A better understanding of the evaporator operation, particularly the phase change phenomenon in gravity field, requires the adoption of an experimental approach allowing the decoupling of different physical mechanisms involved within the porous structure. Thus, it is possible to separately examine the impact of each of the parameters on heat and mass transfers within the porous wick.

As shown in Figs. 3 and 4, the aim of the experimental setup involves representing a flat evaporator section of a capillary two-phase loop. It consists of a porous wick of a copper foam and a grooved brass block. The dimensions of the porous wick are $50 \times 30 \times 15$ mm^3. The experimental configuration also includes a transparent window of sapphire that enables the visualization of the phase change inside the porous wick with a CCD camera (FLIR, *SC*7000). The evaporator is connected to a constant-level reservoir to supply subcooled fluid the wick under the same conditions. The hydrostatic pressure drop is controlled by the elevation Δh, distance between the upper surface of the

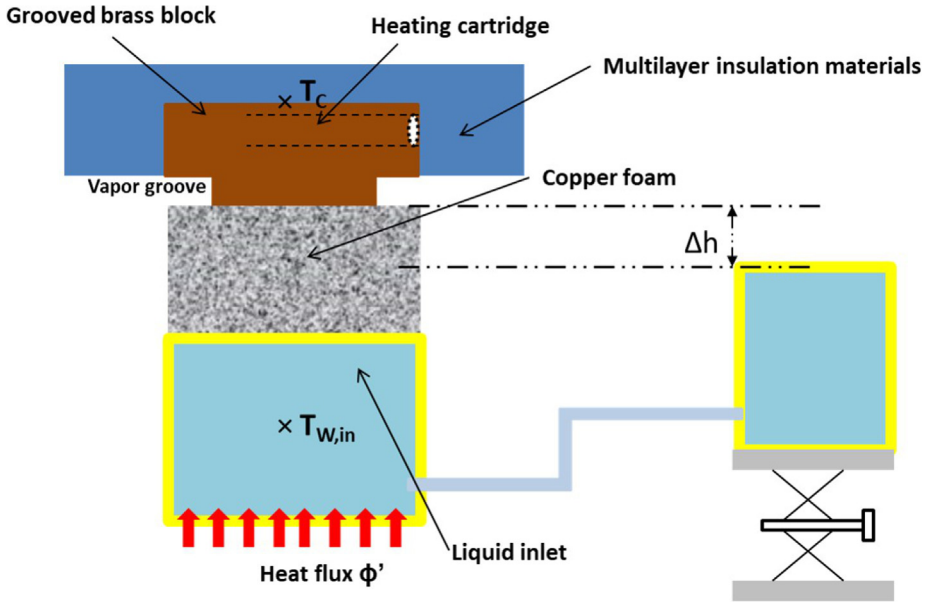

Fig. 3. Experimental setup.

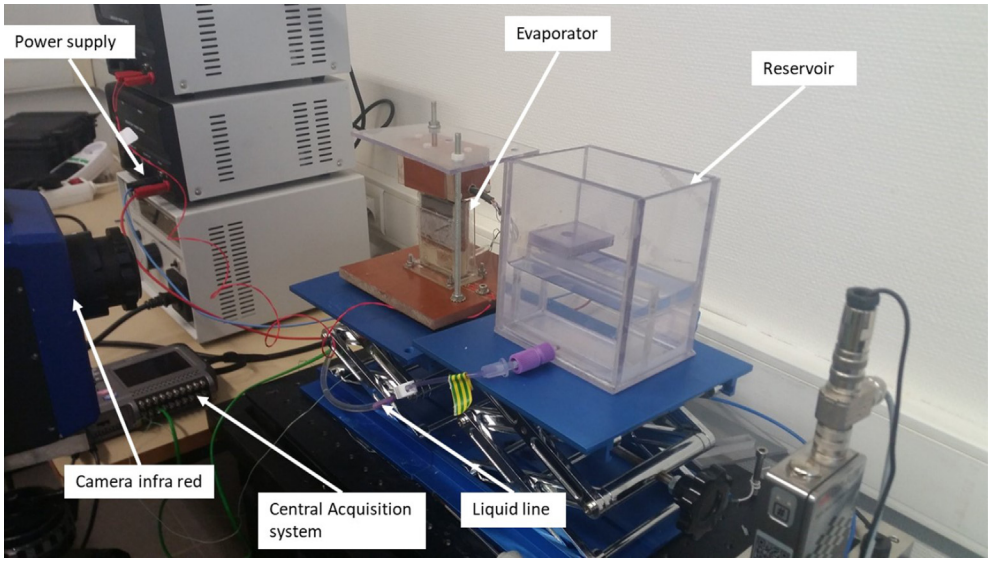

Fig. 4. Experimental setup in real site.

porous structure and water level in the reservoir. The liquid inside the reservoir is at ambient temperature, and thus a heating film is used to heat the liquid before it enters the porous wick to investigate the influence of the subcooling at the wick inlet on the evaporator performance. The upper surface of the porous structure is heated by using a grooved brass block with cartridge heaters. In order to reduce heat losses to the ambient environment, the heating block is thermally insulated with multilayer insulation materials. The system is instrumented with K-type thermocouples to measure the casing temperature T_C and the temperature of the fluid at the wick inlet $T_{W,in}$.

3.2. Boundary conditions

Table 1 summarizes the boundary conditions of the experimental setup.

3.3. Error analysis

The temperatures of the liquid at the wick inlet and the casing are measured by using the K-type thermocouples. Measurement uncertainties are ± 0.5 °C. With respect to the applied power, the relative uncertainty is estimated as 1.1% and it is determined by using the following Equation [27]:

$$\frac{\delta\phi}{\phi} = \sqrt{\left(\frac{\delta V}{V}\right)^2 + \left(\frac{\delta I}{I}\right)^2}$$

3.4. Theoretical study

3.4.1. Momentum balance

In this study, we are interested in examining the phase change in the capillary evaporator. The momentum balance in the porous medium is expressed, in the steady state as follows:

$$\Delta p_{cap} = \rho_\ell g\Delta h + \Delta p_{\ell,W} + \Delta p_{\ell v,W} \quad (2)$$

where $\Delta p_{\ell,W}$ denotes the pressure drop of the liquid phase within the porous structure, $\Delta p_{\ell v,W}$ denotes the pressure drop in the two-phase zone and $\rho_\ell g\Delta h$ denotes the hydrostatic pressure drop. Additionally, the hydrostatic pressure drop in the vapor zone are negligible (the vapor zone thickness and the vapor density are low when compared to those of the liquid phase).

The pressure losses due to the flow of the liquid phase in the porous structure, are evaluated by Darcy's law as follows:

$$\Delta p_{\ell,W} = \frac{\dot{m}\nu_\ell L}{KS_W} \quad (3)$$

where $\dot{m}$ denotes the liquid mass flow rate, ν_ℓ denotes the cinematic viscosity, L denotes the zone liquid length inside the porous wick, K denotes the permeability and S_W denotes the porous material cross-sectional area.

By replacing Eq. (3) in Eq. (2), we obtain the following expression:

$$\dot{m} = \frac{KS_W}{\nu_\ell L}(\Delta p_{cap} - \Delta p_{\ell v,W} - \rho_\ell g\Delta h) \quad (4)$$

3.4.2. Energy balance

The heat load applied to the casing fulfills several functions as follows: a part serves to vaporize the liquid inside the porous structure, a part serves to overheat the liquid and vapor inside the wick, and the last part is lost via conduction toward the porous wick inlet, and this is termed as parasitic heat flux. The energy balance in the capillary evaporator is expressed as follows:

$$\phi = \phi_* + \phi_{sens} + \phi_p$$

where ϕ_* denotes the vaporized heat flux, ϕ_{sens} denotes the sensible heat flux that heats the liquid until it reaches the saturation temperature and ϕ_p denotes the parasitic heat flux. By neglecting the sensible heat flux that overheats the vapor at the outlet of the wick (the vapor temperature leaving the wick is close to the saturation temperature), we obtain the following expression:

$$\phi = \dot{m}[L_v + C_{p_\ell}(T_{sat} - T_{W,in})] + \phi_p$$

The liquid mass flow rate is expressed as follows:

Table 1
Boundary conditions of the experimental setup.

Place of the boundary	Boundary condition
At the upper surface of the porous structure	Heat flux is applied by using grooved brass block with cartridge heaters ϕ
Liquid at the wick inlet	Heat flux is applied by using a heating film ϕ' (see Fig. 3)
Liquid in the reservoir	The fluid is always set at the ambient temperature
Grooves	The groove pressure is set to the atmospheric pressure

$$\dot{m} = \frac{\phi - \phi_p}{[L_v + C_{p_\ell}(T_{sat} - T_{W,in})]} \tag{5}$$

The parasitic heat flux is calculated by using the following equation:

$$\phi_p = \int_{y=0} \lambda_{\text{eff}} \frac{\partial T}{\partial y} dx \tag{6}$$

where λ_{eff} denotes s the effective conductivity of the wick saturated with liquid.

3.4.3. Energy balance for the liquid at the evaporator inlet

The energy balance of the volume of liquid that supplies the wick is expressed as follows:

$$\rho_\ell C_{p_\ell} \Omega_{W,in} \frac{dT_{W,in}}{dt} = \dot{m} C_{p_\ell}(T_{R,o} - T_{W,in}) + \phi_p + \phi' \tag{7}$$

where $\Omega_{W,in}$ denotes the liquid volume at the evaporator inlet prior to entering the porous wick, $T_{R,o}$ denotes the liquid temperature at the reservoir outlet (the ambient temperature), ϕ_p denotes the parasitic heat flux and ϕ' denotes the heat load applied at the bottom of the evaporator.

3.4.4. Heat transfer coefficient

In order to describe the thermal performance of the evaporator, we define the evaporator heat transfer coefficient as follows:

$$h = \frac{\phi}{S(T_C - T_{W,in})} \tag{8}$$

where ϕ denotes the heat flux applied to the evaporator, T_C denotes the casing temperature, $T_{W,in}$ denotes the liquid temperature at the wick inlet and S denotes the contact area between of the input surface.

4. Results and discussion

4.1. Effect of the adverse hydrostatic pressure drop

Fig. 5 shows the temporal evolutions of the casing temperature and the temperature at the inlet of the wick for increasing heat load steps applied uniformly on the evaporator for different values of Δh. During the experiment, the heat flux ϕ' is equal to 2.56 W and the reservoir temperature is set to the ambient temperature. Given the importance of thermal diffusivity and thinness of the casing, the evaporator quickly reacts to any variation in applied thermal load. The casing temperature increases logically with applied power. As shown in Figs. 5c and d, the casing temperature does not stop increasing for $\Delta h = 1.5$ cm and $\Delta h = 2$ cm at the end of the test period, and this iscontrary to the case of $\Delta h = 0.5$ cm and $\Delta h = 1$ cm. The increase in temperature is caused by the penetration of the vapor into the porous wick. This observation is confirmed in Fig. 6 that, zooms in on the part of the wick located under the casing, and shows that the size of the vapor pocket within the porous wick increases with the hydrostatic pressure drop. Specifically, an increase in the hydrostatic pressure drop locally reduces the liquid quantity available to supply the liquid/vapor interface. Consequently, the vapor invades more pores, and the liquid/vapor interface is pushed back downwards the wick. This decreases the heat transfer in the evaporator and increases the temperature of the casing.

As shown in Fig. 7a the temperature of the casing increases with the adverse hydrostatic pressure drop. Based on Eq. (4), an increase inΔh reduces the liquid mass flow rate that supplies the heated surface leading to a large vapor region inside the porous wick. This explains the high overheating of the evaporator wall with an increase in the adverse hydrostatic head Δh.

At the inlet of the wick, the temperature of the liquid depends on that of the liquid coming from the reservoir, parasitic heat flux ϕ_p through the wick and heat flux ϕ' applied to the base of the volume through which the liquid flows (see Eq. (7)). As shown in Fig. 7b, with respect to $\Delta h = 0.5$ cm and $\Delta h = 1$ cm, an increase in the applied power always decreases the liquid temperature at the wick inlet, despite the increase in parasitic heat flux. The drop in temperature is mainly due to the cool liquid coming from the reservoir. Conversely, it is noted that for, $\Delta h = 1.5$ cmand $\Delta h = 2$ cm, the temperature of the liquid at the inlet of the wick first decreases and subsequently increases for high heat loads. This is due to a sudden increase in the parasitic heat flux caused by the significant penetration of the vapor pocket into the porous structure. Given the same reasons as previously described, the liquid temperature at the inlet of the wick increases as a function of the

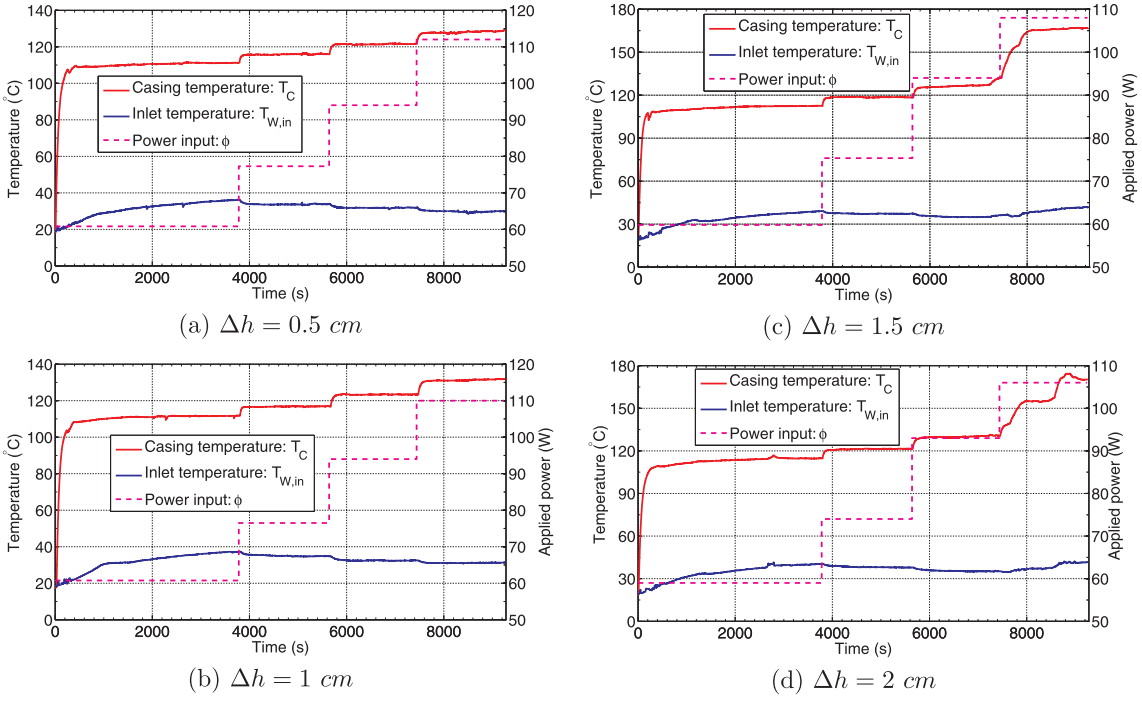

Fig. 5. Effect of the adverse hydrostatic pressure drop.

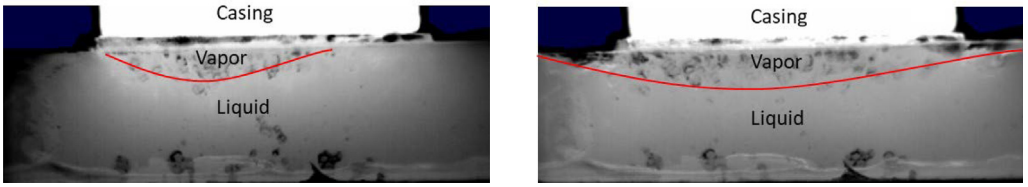

(a) low hydrostatic pressure drop (b) high hydrostatic pressure drop

Fig. 6. Phase change behavior.

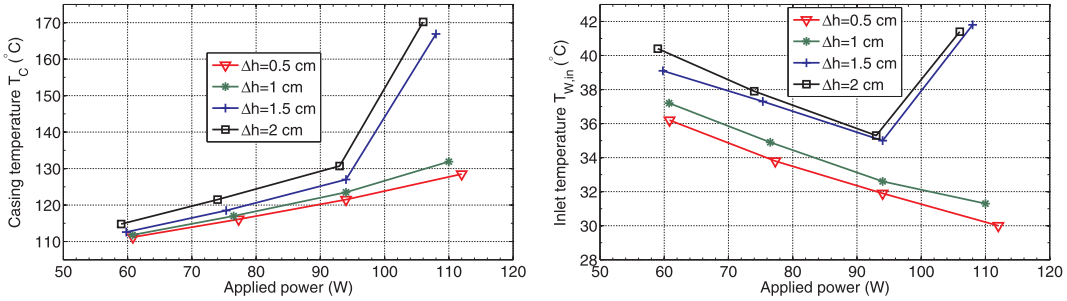

(a) Casing temperature (b) Inlet temperature

Fig. 7. Casing and inlet temperatures at steady state.

adverse hydrostatic head Δh. This is due to the decrease in the mass flow rate of liquid coming from the reservoir.

The variation of the heat transfer coefficient (Eq. (8)) as a function of the hydrostatic pressure drop is shown in Fig. 8. The results indicate that both the heat transfer coefficient and critical heat flux (defined as the heat flux after which the heat transfer coefficient begins to deteriorate rapidly) decreased as Δhincreased. Specifically, with respect to high Δh, the increase in the size of the vapor pocket leads to a significant overheating in the evaporator casing, and this reduces the thermal performance of the evaporator.

4.2. *Effect of subcooling*

In this section, we discuss the influence of subcooling of the liquid entering the wick on the phenomenon of phase change inside the porous medium. Fig. 9 shows the evolution of the casing temperature and the liquid temperature at the inlet of the wick as a function of the heat load applied to the base of the reservoir ϕ' for the same porous structure with the same hydrostatic pressure drop ($\Delta h = 1.5$ cm). It is observed, especially for high heat loads applied to the evaporator, the temperature of the casing decreases when the temperature of the liquid increases at the wick inlet. The amplitude of the subcooling of the liquid at the inlet of the wick significantly influences the parasitic heat flux and sensible heat flux inside the wick. An increase in the temperature of the liquid at the wick inlet decreases the parasitic heat flux and sensible heat flux. Based on Eq. (5), this increases the liquid mass flow rate and reduces the size of the vapor pocket developed inside the porous wick. The location of the liquid/vapor interface near the heated casing decreases its temperature.

The effect of subcooling at the inlet of the wick on the heat transfer coefficient for the same porous structure with the same hydrostatic pressure drop is illustrated in Fig. 10. The heat transfer coefficient increases with the decrease in the subcooling at the inlet of the wick. The behavior is explained by the fact that an increase in the temperature at the inlet of the wick (as shown in Fig. 9 and Eq. (8)) decreases the temperature difference between the evaporator casing and liquid at the inlet of the wick.

4.3. *Effect of porous medium*

In this section, we focus on the impact of porosity and mean pore diameter on heat and mass transfers into the porous wick. Table 2 shows the properties of the materials of the two porous wicks that exhibits different porosities and mean pore diameters.

Porosity is a crucial parameter that significantly impacts both the fluid flow and heat transfer in the wick. Specifically, an increase in the porosity increases the amount of fluid contained in the wick that, decreases the effective thermal conductivity (the liquid or vapor thermal conductivity is lower than that of the structure of the solid matrix). Conversely, an increase in porosity increases permeability, and this is directly related to the fluid flow inside the porous wick (see Eq. (3)). The pore diameter also directly impacts the maximum capillary pressure. Based on Eq. (1) an increase in pore diameter decreases the maximum capillary pressure achievable by the wick. A decrease in the pore diameter leads to high pumping in the wick although it increases pressure losses.

Fig. 11a describes the variation of the casing temperature of the metal frame as a function of the applied power for two porous wicks. It is observed that the casing temperature for **wick** #1 is lower than that of **wick** #2 for a low applied heat load, and subsequently it suddenly increases for a high applied heat load. The behavior for the low applied heat load is explained by the fact that **wick** #1 exhibits a high effective

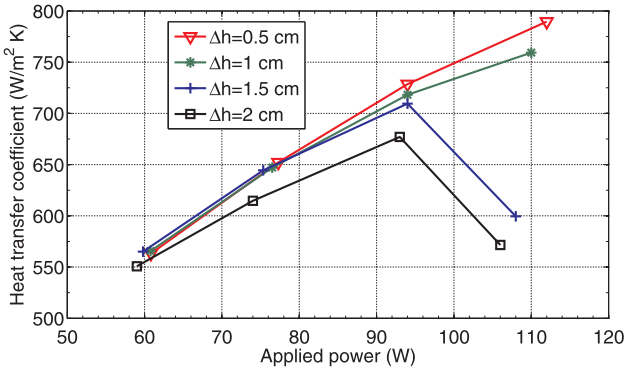

Fig. 8. Effect of the adverse hydrostatic on the heat transfer coefficient.

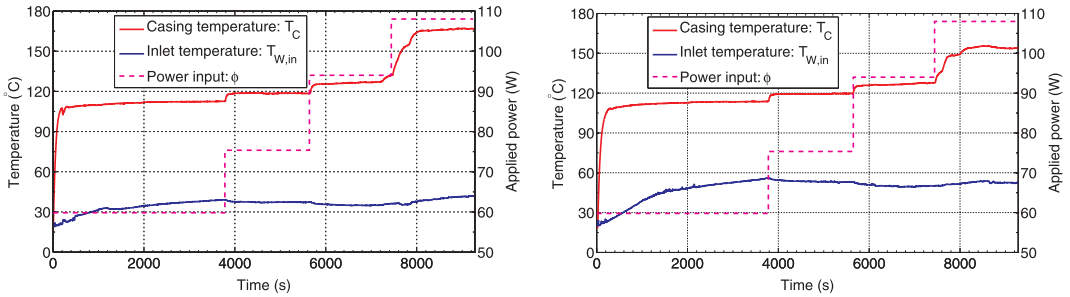

(a) $\phi_2 = 2.56\ W$ (b) $\phi_2 = 5.52\ W$

Fig. 9. Effect of the subcooling at the wick inlet for $\Delta h = 1.5$ cm.

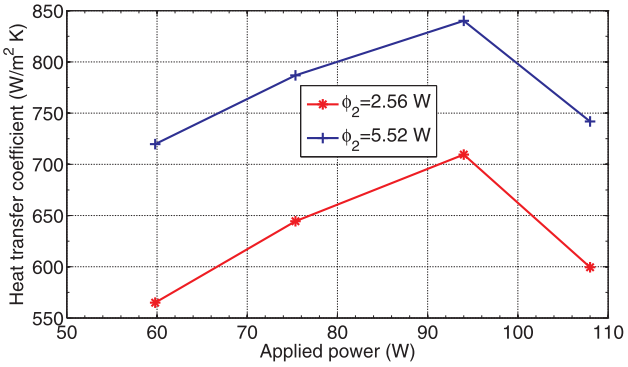

Fig. 10. Effect of the subcooling on the heat transfer coefficient for $\Delta h = 1.5$ cm.

Table 2
Porous media properties.

	wick #1	**wick** #2
Material	Copper foam	Copper foam
Mean pore diameter (mm)	0.423	0.635
Porosity (%)	90	96
Permeability (m^2)	7.24 10^{-8}	1.238 10^{-6}
Effective thermal conductivity (W/mK)	39.608	16.24

thermal conductivity (the high thermal conductivity aids in efficiently transferring heat to the evaporating menisci in the capillary structure by conduction) and a high capillary pressure. Specifically, low pore diameters provide sufficient capillary pressure to maintain a stable liquid/vapor interface within the wick and to compensate for the pressure drop. The sudden increase in the casing temperature during regime II for **wick** #1 is explained by the vapor breakthrough at the inlet of the wick. Specifically, an increase in the applied power increases the significance of the pressure drop in the vapor and liquid phases for **wick** #1 when compared to that of **wick** #2 (the permeability of **wick** #1 is lower than that of **wick** #2). This increases the overheating of the casing causing and decreases the thermal performance.

Fig. 11b shows the evolution of the temperature at the inlet of the wick as a function of the applied power for the two porous wicks with the adverse hydrostatic head $\Delta h = 0.5$ cm. The temperature at the inlet for **wick** #1 exceeds that for**wick** #2. Specifically, **wick** #1 exhibits a high effective thermal conductivity whencompared to that of **wick** #2, and this increases the parasitic heat flux based on Eq. (6).

The effect of porosity and average pore diameter on the heat transfer coefficient is shown in Fig. 12. The heat transfer coefficient of the evaporator containing **wick** #1 significantly exceeds that of **wick** #2 when the applied power is lower than 82 W. The phenomenon is explained by the low effective thermal conductivity and the high porosity of **wick** #2. With respect to a heat load exceeding 82 W, its thermal performance suddenly decreases due to the vapor breakthrough toward the wick inlet. It is noted that the critical heat flux of the evaporator containing **wick** #2 exceedsthat of **wick** #1. Consequently, we can conclude that it exists optimal values of porosity and pore diameter leading to both the best heat transfer coefficient and the largest critical heat flux. These results are in accordance with the numerical results of Mottet [28].

5. Conclusion

The study experimentally investigated the phenomenon of phase change in a porous medium of a capillary evaporator. Based on the experimental results on the effect of the adverse hydrostatic pressure drops, the subcooling at the wick inlet and the properties of the material, the following conclusions were obtained:

1. The variation in the adverse hydrostatic head from $\Delta h = 0.5$ cm to $\Delta h = 2$ cm increases the evaporator temperature by 5 °C for low heat loads and 40 °C for high heat loads.
2. The heat transfer coefficient and critical heat flux decrease with an increase in the adverse hydrostatic pressure drop due to the vapor breakthrough toward the wick inlet.

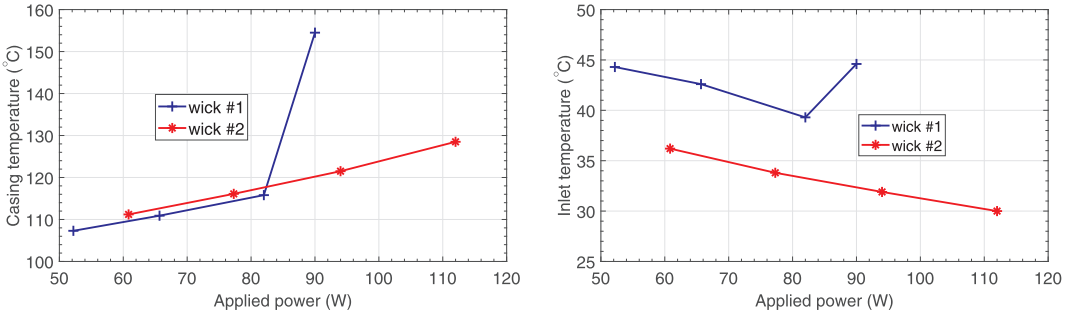

(a) Casing temperature (b) Inlet temperature

Fig. 11. Effect of the wick properties on the casing and inlet temperatures.

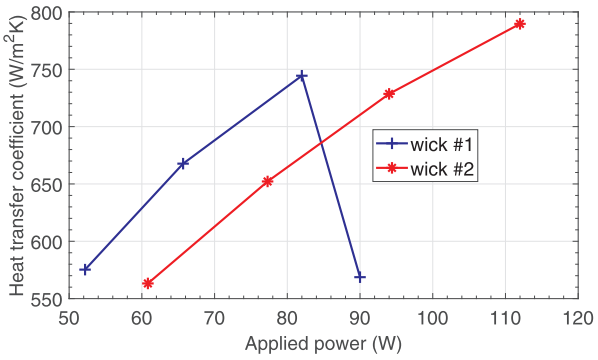

Fig. 12. Effect of the wick properties on the heat transfer coefficient.

3. The vapor pocket developed inside the porous wick increases with the adverse hydrostatic pressure drop, which explains the significant degradation of the evaporator thermal performance.
4. Although subcooling is necessary to avoid the evaporator deprime resulting from the formation of bubbles at the inlet of the wick, the results indicate that its increase reduces the thermal performance of the capillary performance. Thus, an optimal subcooling occurs and leads to the best thermal performance of the capillary evaporator before its performance deteriorates.
5. The porosity and average pore diameter significantly impact the phase change phenomenon and heat transfer coefficient. It exists optimal values of porosity and pore diameter to maximize the heat transfer coefficient and critical heat flux.

Acknowledgements

This work has been achieved within the framework of CE2I project (Convertisseur d'Énergie Intégré Intelligent). CE2I is co-financed by European Union with the financial support of European Regional Development Fund (ERDF), French State and the French Region of Hauts-de-France.

References

[1] R. Boubaker, V. Platel, Dynamic model of capillary pumped loop with unsaturated porous wick for terrestrial application, Energy 111 (2016) 402–413.
[2] N. Blet, Y. Bertin, V. Ayel, C. Romestant, V. Platel, Experimental analysis of a capillary pumped loop for terrestrial applications with several evaporators in parallel, Appl. Therm. Eng. 93 (2016) 1304–1312.
[3] Y. Maydanik, Loop heat pipes, Appl. Therm. Eng. 25 (5) (2005) 635–657.
[4] Y. Maydanik, V. Pastukhov, M. Chernysheva, Development and investigation of a loop heat pipe with a high heat-transfer capacity, Appl. Therm. Eng. 130 (2018) 1052–1061.
[5] T. Kaya, J. Goldak, Numerical analysis of heat and mass transfer in the capillary structure of a loop heat pipe, Int. J. Heat Mass Transfer 49 (2006) 3211–3220.
[6] A. Demidov, E. Yatsenko, Investigation of heat and mass transfer in the evaporation zone of a heat pipe operating by the 'inverted meniscus' principle, Int. J. Heat Mass Transfer 37 (14) (1994) 2155–2163.
[7] X.M. Huang, W. Liu, A. Nakayama, S.W. Peng, Modeling for heat and mass transfer with phase change in porous wick of CPL evaporator, Heat Mass Transfer 41 (2005) 667–673.
[8] Y. Xuan, K. Zhao, Q. Li, Investigation on heat and mass transfer in a evaporator of a capillary-pumped loop with the lattice boltzmann method: Pore scale simulation, Transp. Porous Media 89 (2011) 337–355.
[9] M. Nishikawara, H. Nagano, Numerical simulation of capillary evaporator with microgap in a loop heat pipe, Int. J. Therm. Sci. 102 (2016) 39–46.
[10] L. Mottet, M. Prat, Numerical simulation of heat and mass transfer in bidispersed capillary structures: application to the evaporator of a loop heat pipe, Appl. Therm. Eng. 102 (2016) 770–784.
[11] R. Boubaker, V. Platel, A. Berges, M. Bancelin, E. Hannezo, Dynamic model of heat and mass transfer in an unsaturated porous wick of capillary pumped loop, Appl. Therm. Eng. 76 (2015) 1–8.
[12] R. Boubaker, V. Platel, Vapor pocket behavior inside the porous wick of a capillary pumped loop for terrestrial application, Appl. Therm. Eng. 84 (2015) 420–428.
[13] R. Boubaker, V. Platel, S. Harmand, A numerical comparative study of the effect of working fluids and wick properties on the performance of capillary pumped loop with a flat evaporator, Appl. Therm. Eng. 100 (2016) 564–576.
[14] Z. Wan, J. Liu, J. Wan, Z. Tu, W. Liu, An overall numerical investigation on heat and mass transfer for miniature flat plate capillary pumped loop evaporator, Thermochim. Acta 518 (1) (2011) 82–88.
[15] S.-Y. Wu, X.-F. Zheng, L. Xiao, Phase change heat transfer characteristics of porous wick evaporator with bayonet tube and alkali metal as working fluid, Int. J. Therm. Sci. 126 (2018) 152–161.
[16] K.H. Le, A. Kharaghani, C. Kirsch, E. Tsotsas, Pore network simulations of heat and mass transfer inside an unsaturated capillary porous wick in the dry-out regime, Transp. Porous Media 114 (3) (2016) 623–648.
[17] M.A. Chernysheva, Y.F. Maydanik, 3d-model for heat and mass transfer simulation in flat evaporator of copper-water loop heat pipe, Appl. Therm. Eng. 33-34 (2012) 124–134.
[18] J. Li, G. Peterson, 3d heat transfer analysis in a loop heat pipe evaporator with a fully saturated wick, Int. J. Heat Mass Transfer 54 (1) (2011) 564–574.
[19] X. Zhang, X. Li, S. Wang, Three-dimensional simulation on heat transfer in the flat evaporator of miniature loop heat pipe, Int. J. Therm. Sci. 54 (2012) 188–198.
[20] A.A. Pozhilov, D.K. Zaitsev, E.M. Smirnov, A.A. Smirnovsky, Numerical simulation of heat and mass transfer in a 3d model of a loop heat pipe evaporator, St. Petersburg Polytech. Univ. J.: Phys. Math. 3 (3) (2017) 210–217.
[21] L. Mottet, T. Coquard, M. Prat, Three dimensional liquid and vapour distribution in the wick of capillary evaporators, Int. J. Heat Mass Transfer 83 (2015) 636–651.
[22] Q. Liao, T.S. Zhao, Evaporative heat transfer in a capillary structure heated by a grooved block, J. Thermophys. Heat Transfer 13 (1999) 126–133.
[23] Q. Liao, T.S. Zhao, A visual study of phase-change heat transfer in a two- dimensional porous structure with a partial heating boundary, Int. J. Heat Mass Transfer 43 (2000) 1089–1102.
[24] X.L. Cao, P. Cheng, T.S. Zhao, Experimental study of evaporative heat transfer in sintered copper bidispersed wick structures, J. Thermophys. Heat Transfer 16 (2002) 547–552.
[25] T. Coquard, Coupled heat and mass transfer in an element of a capillary evaporator (in French) (Ph.D. thesis), Institut National Polytechnique de Toulouse, Toulouse, France, 2006.
[26] K. Odagiri, M. Nishikawara, H. Nagano, Microscale infrared observation of liquid-vapor interface behavior on the surface of porous media for loop heat pipes, Appl. Therm. Eng. 126 (2017) 1083–1090.
[27] R.J. Moffat, Describing the uncertainties in experimental results, Exp. Thermal Fluid Sci. 1 (1) (1988) 3–17.
[28] L. Mottet, Simulations of heat and mass transfer within the capillary evaporator of a two-phase loop (Ph.D. thesis), Institut National Polytechnique de Toulouse, Toulouse, France, 2016.